Archives of Toxicology (2020) 94:3503–3514
https://doi.org/10.1007/s00204-020-02845-9

IN VITRO SYSTEMS

In vitro stress response induced by sulfur mustard in lung fibroblasts NHLF and human pulmonary epithelial cells A-549

Petr Jost[1] · **Lubica Muckova**[1] · **Jaroslav Pejchal**[1]

Received: 28 April 2020 / Accepted: 9 July 2020 / Published online: 17 July 2020

Abstract

Sulfur mustard [bis(2-chloroethyl) sulfide; SM] is a highly poisonous chemical warfare agent. The mechanism of its cytotoxicity affects several pathways, which cause cell damage or death. The main organ affected in case of exposure to both aerosol and vapor is lungs. The present study focuses on time- and concentration-dependent changes in human lung fibroblasts NHLF and lung epithelial cell line A-549. The cells were treated with SM at the concentrations of 5, 10 and 100 µM and signs of stress response were evaluated during 1–72 h post-treatment. Parameters for testing included cell viability and morphology, loss of transmembrane mitochondrial potential, apoptosis, oxidative stress, changes in the cell cycle, and ATM kinase activation. The cytotoxic effect of SM resulted in a time-dependent decrease in viability of A-459 associated with apoptosis more markedly than in NHLF. We did not observe any generation of reactive oxygen species by SM. SM at concentrations of 5 and 10 µM induced the S-phase cell cycle arrest at both cell lines. On the other hand, 100 µM caused nonspecific cell cycle arrest. ATM kinase was activated transiently. The results indicate that NHLF cells are less prone to toxic damage by SM in case of cell viability, apoptosis and loss of transmembrane mitochondrial potential. The analysis provides a time-related cytotoxic profile of A-549 and NHLF cells for further investigation into the prevention of SM toxic effects and their potential treatment.

Article Highlights

(1) Sulfur mustard induced the time- and concentration-dependent cytotoxic effects on both A-549 cells and lung fibroblast NHLF.
(2) Sulfur mustard at concentrations of 5 and 10 µM caused cell cycle arrest in S-phase, whereas 100 µM inhibited cell cycle completely.
(3) Loss of mitochondria potential occurred with the latency of several hours.
(4) SM induced transient activation of ATM kinase.
(5) The DCFH-DA fluorescent probe did not confirm the generation of ROS.

Keywords Sulfur mustard · Cytotoxicity · Apoptosis · Cell cycle · S-phase arrest · A-549 cell line · Lung fibroblasts NHLF

Introduction

Sulfur mustard [SM; bis(2-chloroethyl) sulphide] is a cytotoxic and cytostatic agent with a blistering effect on human skin. The respiratory tract is a vital target organ as well as the route of intoxication. Inhalation exposure to SM is often lethal or it could become a source of chronic symptoms and disability in long-term survivors (Seagrave et al. 2010; Weinberger et al. 2011). Elucidation of the mechanism of SM toxicity has, therefore, been at the center of intensive research. Several hypotheses explaining the molecular basis of SM action have been postulated (Pilatte and Lison 1994; Tewari-Singh et al. 2010; Sawyer et al. 2010; Inturi et al. 2011; Long et al. 2016). SM causes damage to nucleic acids, induces glutathione depletion, oxidative stress, lipid peroxidation, and protein dysfunction. Altogether, this results in

✉ Petr Jost
petr.jost@unob.cz

[1] Department of Toxicology and Military Pharmacy, Faculty of Military Health Sciences, University of Defence in Brno, Trebesska 1575, 500 01 Hradec Kralove, Czech Republic

the activation of various mechanisms, which subsequently participate in the final cytopathology (Imani et al. 2015).

To date, it is clear from recent studies that direct interaction of SM with DNA bases leads to the formation of alkyl adducts, preferably on *N*7 guanine and *N*3 adenine, or cross-links, the pathological couplings of two DNA bases on the complementary DNA strands. Genotoxic stress represents a critical trigger of several signaling pathways in the cell regulating DNA damage response, energy metabolism, cell cycle, or apoptosis (Long et al. 2016). There is a delay in the cellular response to SM exposure. Therefore, a time-course analysis is essential for the elucidation of complex SM cytotoxic action.

The purpose of our study is to evaluate the time- and concentration-dependent changes in cellular pathophysiology after SM exposure. We aimed to investigate selected processes employed on multiple levels of cellular response. Two human pulmonary origin cell lines, including fibroblasts (NHLF; normal human lung fibroblasts) and human lung epithelial cells A-549, were used as an in vitro experimental model. The cells were treated with SM at the concentrations of 5, 10 and 100 µM. We investigated nine cellular parameters during the period of 1–72 h.

Material and methods

Cells and cell culture

NHLF were obtained from Lonza (Lonza Walkersville, Inc., MD, USA). A-549 cell line was purchased from the American Type Culture Collection (ATCC, Manassas, VA, USA). Cells were grown in Dulbecco's modified Eagle's medium (DMEM) supplemented with 10% fetal bovine serum (FBS) and 1% antibiotic–antimycotic solution (all from Biosera, Nuaillé, France) at 37 °C in an atmosphere of 5% CO_2 and 85–90% air humidity. At approximately 80% confluence, the cells were routinely passaged by trypsinization. NHLF cells between passages 3–10 were used for experiments.

Both, NHLF and A-549 cells were tested on *Mycoplasma sp*. contamination using MycoAlert PLUS Mycoplasma detection kit (Lonza Walkersville, Inc.) according to the manufacturer's instructions with negative results.

Chemicals and treatment

SM was obtained from Military Facility Service VOS 072 (≥ 98% purity determined by GC–MS; Zemianske Kostoľany, Slovak Republic). Dimethyl sulfoxide (DMSO) was purchased from Sigma–Aldrich (Saint Louis, MO, USA). A stock solution of 400 mM SM in DMSO was stored at − 20 °C for up to one month. The final concentration of SM in the culture medium was 5, 10 or 100 µM. Measurements were performed with cells exposed to SM for 1, 4, 8, 16, 24, 36, 48, and 72 h. We utilized DMSO in the equivalent volume to treat negative controls. The final concentration of DMSO in the culture medium did not extend 0.25% in all experiments.

Cell viability assays

Three different viability assays were used for evaluation of SM cytotoxicity, including 3-(4,5-dimethylthiazol-2-yl)-2,5-diphenyltetrazolium bromide (MTT, Sigma-Aldrich) reduction assay, calcein-acetoxymethyl ester (calcein-AM, Sigma-Aldrich) assay, and real-time impedance-based cell analysis (Acea Bioscience Inc., San-Diego, USA).

MTT assay

Cells were plated into 96-well plates (TPP, Trasadingen, Switzerland) at a density of 4 or 8×10^3 cells per well according to the treatment period and incubated at 37 °C in a CO_2 incubator overnight. At the indicated time of analysis, the medium was aspirated and replaced by fresh medium containing 1/10 (v/v) MTT stock solution (5 mg/mL) in each well. The plate was incubated at 37 °C in a CO_2 incubator for 40 min. The medium was then aspirated and the purple formazan was dissolved in 100 µL of DMSO. The plate was shaken and the optical density of each well was measured on a Synergy two Multi-Mode Microplate Reader (BioTek Instruments, Inc., Winooski, VT, USA) at 570 nm. The cell viability was expressed as a percentage of the untreated control. The results were obtained from three independent experiments. Each measurement was performed in a replicate $n = 4$.

Calcein-AM assay

Cells were plated into a black-walled 96-well plate at the density of 4 or 8×10^3 cells per well and incubated at 37 °C in a CO_2 incubator overnight. In the selected time intervals, the medium was aspirated and cells were washed by DPBS with calcium and magnesium (Hyclone Laboratories, Logan, UT, USA. DMEM without phenol red (100 µL; BioConcept, Allshwill, Switzerland) was added in each well containing 5 µM calcein-AM. The plate was then incubated at 37 °C in a CO_2 incubator for 50 min. After incubation, the calcein-AM was aspirated and cells were lysed by 1% SDS (Sigma-Aldrich) in distilled water. The fluorescence was measured on the Synergy two Multi-Mode Microplate Reader (BioTek) with excitation wavelength 485 nm and the emission wavelength of 530 nm. The cell viability was expressed as a percentage of the untreated control. The results were obtained from three independent experiments. Each measurement was performed in a replicate $n = 4$.

Real-time cell analysis of SM toxicity

E-plates 96 (Acea Bioscience Inc., San-Diego, USA) were filled with 50 µL of DMEM per well to measure background signal. Cell suspension (140 µL; concentration 8×10^3/well) was then added and the E-plate 96 was left at room temperature for 20 min to attach cells homogeneously. E-plate 96 was then returned to the CO_2 incubator, connected with the monitoring device, and monitored overnight. The next day, the cells were exposed to SM and E-plate was linked back to the device. The electrical impedance signal expressed as a dimensionless normalized cell index (NCI) was automatically recorded every 60 min for the next 168 h (7 days) to obtain time-dependent cell response curves. Each measurement was carried out in a replicate $n = 4$.

Apoptosis

The determination of apoptotic cells was conducted by Muse Annexin V and Dead Cell Kit (Merck-Millipore, Darmstadt, Germany). The cells were plated into 6-well plates (one plate for each time interval) at the density of 1.5×10^5 cells per well, allowed to adhere at 37 °C in the CO_2 incubator overnight and then treated with SM. At the indicated time, 100 µL of trypsinized cell suspension was mixed with 100 µL assay reagent. Afterwards, the samples were incubated for 30 min and analyzed by Muse Cell Analyser (Merck-Millipore) according to the manufacturer's instructions. The results were obtained from three independent experiments, 5000 events per sample were analyzed.

Mitochondrial membrane potential

Changes in mitochondrial membrane potential were assayed using the Muse MitoPotential Kit (Merck-Millipore). The cells were plated into 6-well plates (one plate for each time interval) at the density of 1.5×10^5 cells per well, allowed to adhere at 37 °C in the CO_2 incubator overnight and then treated with SM. At the indicated time, the cells were harvested and 100 µL of the sample was mixed with 95 µL of MitoPotential dye working solution and incubated at 37 °C for 20 min. After the addition of Muse MitoPotential 7-AAD dye (dead cell detection) and incubation for 5 min, changes were assessed using fluorescent intensities of both dyes. The results were obtained from three independent experiments. The Muse Cell Analyser analyzed 5000 events per sample.

Cellular morphology

Cells were plated into 6-well plates (1.5×10^5 cells/well) and allowed to adhere at 37 °C in a CO_2 incubator overnight. The cells were treated with 100 µM SM. Microphotographs were taken using light invert phase-contrast microscope Nikon Eclipse TS100-F with a digital camera (Nikon, Tokyo, Japan) under 200 × magnifications.

Cell cycle analysis

Cell cycle distribution was analyzed by Muse Cell Cycle Kit (Merck-Millipore). Cells were plated into 6-well plates (one plate for each time interval) at the density of 1.5×10^5 cells per well, allowed to adhere at 37 °C in a CO_2 incubator overnight and then treated with SM. After the treatment, the cells were collected by trypsinization, washed in PBS, fixed in 70% ethanol, and stored at − 20 °C until analyses. Fixed cells were then washed with PBS and stained with cell cycle reagent (Muse Cell Cycle Reagent, Merck-Millipore) at room temperature in the dark for 30 min. The results were obtained from three independent experiments, 5000 events per sample were analyzed by the Muse Cell Analyser.

Measurement of intracellular reactive oxygen species (ROS) level

Intracellular ROS were detected by 2,7-dichlorodihydrofluorescein diacetate (DCFH-DA, Cayman Chemical Company, Ann Arbor, MI, USA). DCFH-DA is a nonfluorescent dye. It can be converted to the fluorescent 2,7–dichlorofluorescein (DCF) by intracellularly generated ROS. For the assay, the cells were plated into black 96-well plates at density 4 or 8×10^3 cells per well and incubated at 37 °C in a CO_2 incubator overnight. After the treatment with SM or *tert*-butylhydroperoxide (Sigma–Aldrich) as a positive control, the cells were incubated with 10 µM DCFH-DA at 37 °C for 30 min. Fluorescence intensity was measured by a Synergy 2 Multi-Mode Microplate Reader (excitation 488 nm, emission 530 nm). The results were obtained from three independent experiments. Each measurement was carried out in a replicate $n = 4$.

ATM activation assay

The phosphorylated form of ATM kinase was detected by Muse Multi-color DNA Damage Kit (Merck-Millipore). The cells were plated into 6-well plates (one plate for each time interval) at the density of 1.5×10^5 cells per well, allowed at 37 °C in the CO_2 incubator to adhere overnight and then treated with SM. At the indicated time, 100 µL of trypsinized cells were resuspended in a mixture of 50 µL of assay buffer and 50 µL fixation buffer and allowed for 10 min on ice. Then, the cells were permeabilized in 100 µL ice-cold permeabilization buffer for 10 min, resuspended in 90 µL assay buffer and stained with anti-phospho-ATM (Ser1981)-PE conjugated antibodies for 30 min at room temperature in the dark. The excess of dye was washed out with ice-cold assay buffer. Cells were then analyzed by Muse Cell

Analyzer (Merck-Millipore) according to the manufacturer's instructions. The results were obtained from three independent experiments, 5,000 events per sample were analyzed.

Data analysis

Statistical analysis was performed using GraphPad Prism version 5.04 for Windows (GraphPad Software, San Diego, CA, USA) by two-way analysis of variance (ANOVA) and Bonferroni posthoc test to compare SM exposed groups with control. The level of significance was evaluated at levels $p \leq 0.05$ (*), $p \leq 0.01$ (#) and $p \leq 0.001$ (&). Data in graphs represent a mean ± standard error of the mean (SEM). Cell microphotographs were not statistically evaluated.

Results

Cell viability

MTT assay

The colorimetric MTT assay was used for the detection of the viability of cells treated with SM at concentrations of 5, 10 and 100 µM for 1–72 h period. The response of both lung fibroblasts NHLF and A-549 cells was strictly concentration-dependent with time course progression (Fig. 1).

In NHLF, 5 µM SM induced the significant decrease in cell viability at 36, 48 and 72 h. At the concentration of 10 µM, the cell viability decreased from 24 h onwards. 100 µM of SM caused significant loss of cell viability at 4, 8, 16, 24, 36, 48, and 72 h (Fig. 1a).

In A-549 cells, 5 µM SM significantly reduced cell viability at intervals from 16 to 72 h. At 10 µM, it decreased in the same period. SM at the concentration of 100 µM caused significant loss of cell viability from 8 h onwards (Fig. 1b).

Calcein-AM assay

The fluorescence-based calcein-AM assay was used for measuring cell viability on the principle of intact cell membranes in the living cells.

In NHLF, cell viability significantly decreased at 5 µM at 36, 48 and 72 h. At 10 µM, it dropped at identical time points. The concentration of 100 µM SM reduced cell viability at 16, 24, 36, 48, and 72 h (Fig. 2a).

When compared to NHLF, we found significantly decreased viability of A-459 cells at the concentration of 5 and 10 µM at 24, 36, 48, and 72 h. 100 µM caused a reduction in viability at 16 h onwards (Fig. 2b).

Electric impedance-based cell viability assay

Cytotoxicity of SM was also monitored by a label-free electric impedance-based method every 60 min for 192 h. Cell treatment was performed after overnight incubation (black arrows in the graphs, Fig. 3).

In NHLF cells, the control curve reached a maximum at 80 h. Then, the NCI slowly decreased. At 5 µM, NCI transiently increased above the control curve at 6–30 h post-treatment. It was followed by a plateau phase, causing a significant decrease of NCI at 42 h when compared to control. After that, proliferation renewed, reaching the control curve at 96 h. SM at 10 µM caused a similar effect as described above. The significant transient rise of NCI was recorded from 9 to 25 h after SM treatment. Then, it started to decrease. When compared with control, it became significantly lower at 37 h. Afterwards, the proliferation renewed, reaching the control curve 105 h after

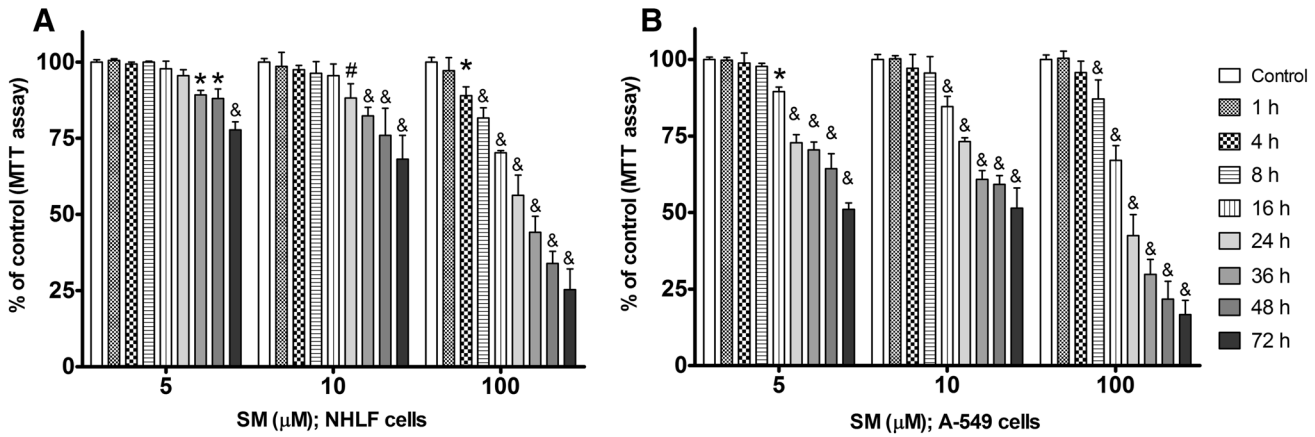

Fig. 1 Changes in the viability of lung fibroblasts NHLF (**a**) and A-549 cells (**b**) treated with 5, 10 and 100 µM of SM for 1–72 h. Cell viability was determined by the colorimetric MTT assay. The data are expressed as mean ± SEM, $n = 4$. $^{*}p \leq 0.05$, $^{\#}p \leq 0.01$ and $^{\&}p \leq 0.001$ when compared with the control

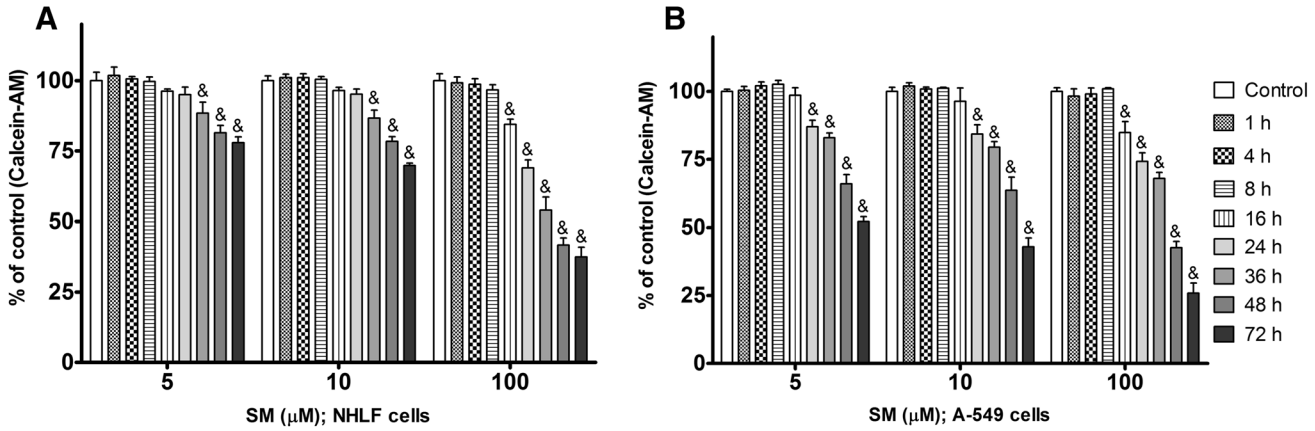

Fig. 2 Changes in the viability of lung fibroblasts NHLF (**a**) and A-549 cells (**b**) treated with 5, 10 and 100 μM of SM for 1–72 h. Cell viability was determined by the fluorescence-based method with calcein-AM. The data are expressed as mean ± SEM, $n = 4$. $^{\&}p \leq 0.001$ when compared with the control

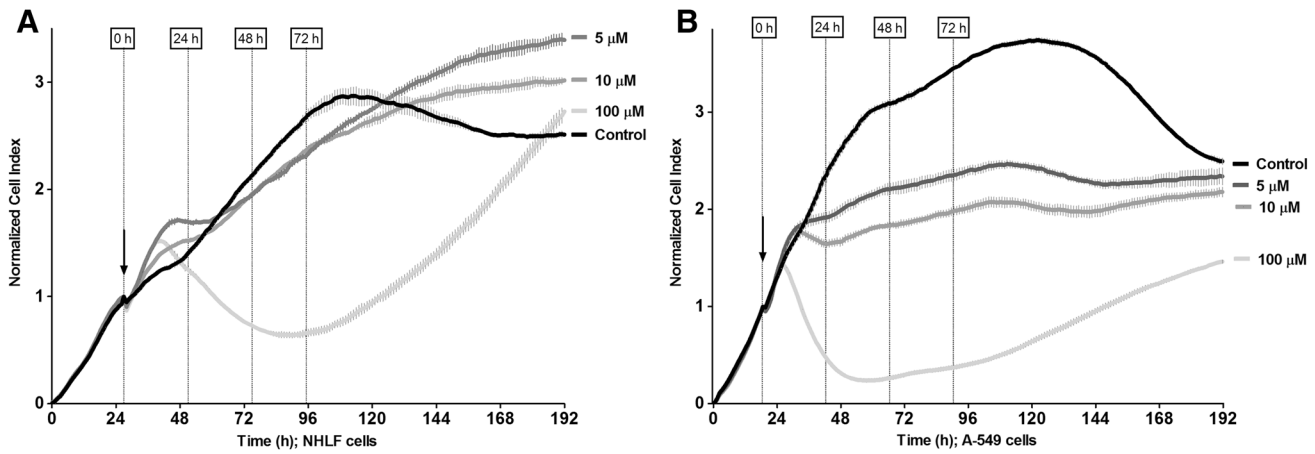

Fig. 3 Electric impedance-based analysis of SM cytotoxicity. NHLF (**a**) and A-549 (**b**) cells were seeded in a 96-well E-plate (8×10^3 cells/well). Cells were left to attach and grow overnight and then were exposed to SM (black arrow). Cell adherence and proliferation were monitored every 60 min for 192 h. Figures **a** and **b** show the time-dependent alteration of the normalized cell index at concentrations of 5, 10 and 100 μM SM. The data show the representative result of three independent experiments with similar results. Grey bars represent mean ± SEM, $n = 4$

the SM treatment. At 100 μM, NCI transiently increased 6–18 h post-treatment. Then, it sharply decreased in the 23–63 h interval. Finally, it started to rise at 66 h, crossing the control curve at 157 h.

The control curve of A-549 cells reached a maximum of NCI at 104 h. At the concentration of 5 and 10 μM, the rise of NCI significantly decelerated at 20 h and 17 h after the SM treatment, respectively, demonstrating only limited growth during the whole observation period. The concentration of 100 μM caused a sharp, significant decrease of NCI after 10 h, reaching a minimum at 37 h post-treatment. Then, A-549 cells restored cell proliferation, which was associated with increasing NCI.

Apoptosis by microcapillary flow-cytometry

NHLF cells did not show significant induction of apoptosis at both 5 and 10 μM during the observation period. At 100 μM SM, we found an increase of early apoptotic cell population at 72 h, while the percentage of the late apoptotic cells was significantly higher than in control at 48 and 72 h (Fig. 4a).

A-549 cells show a more pronounced time-dependent response. SM at 5 μM induced an increase of late apoptotic cells at 36, 48 and 72 h. The concentration of 10 μM increased the population of early apoptotic cells at 24, 36, 48, and 72 h, while the representation of late apoptotic

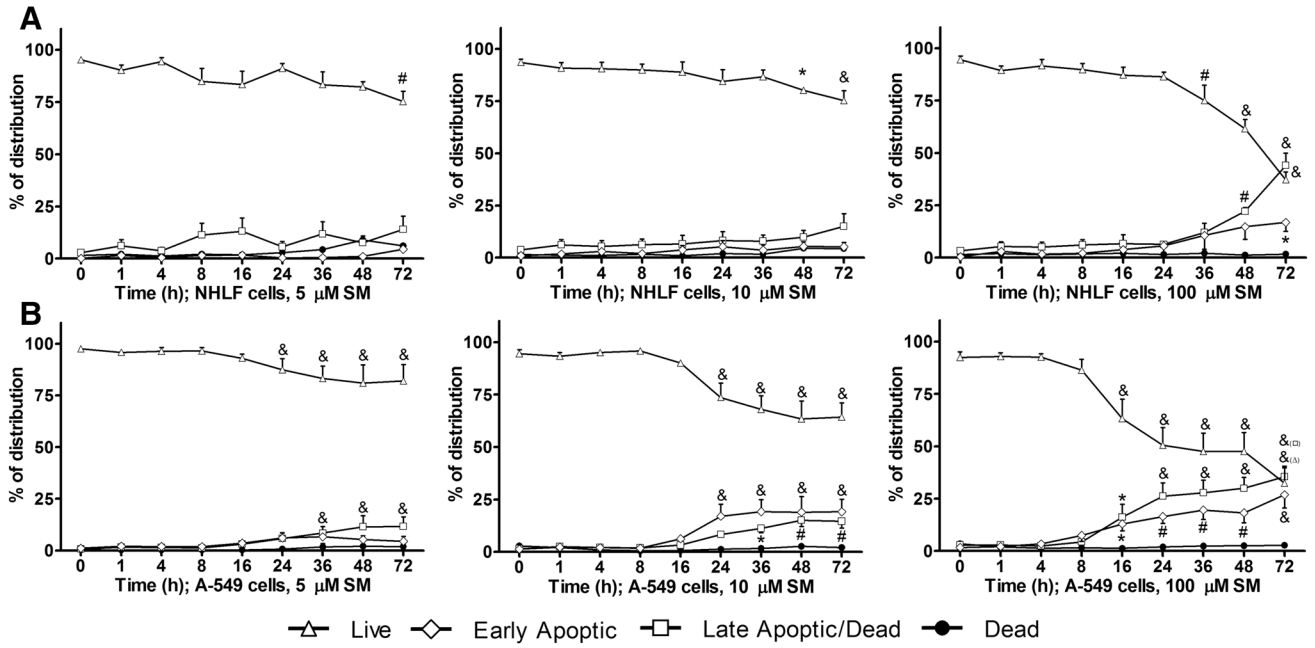

Fig. 4 Induction of apoptosis by SM in (**a**) human lung fibroblasts NHLF and (**b**) A-549 cells during the 1–72 h period. Apoptotic cell distribution was measured by annexin V/propidium iodide-based assay kit by microcapillary flow cell analyzer. The data are expressed as mean ± SEM, from three independent experiments. $^{*}p \leq 0.05$, $^{\#}p \leq 0.01$ and $^{\&}p \leq 0.001$ when compared with the control (0)

cells was significantly higher at 36, 48 and 72 h. The most progressive changes were induced by 100 μM of SM. The population of early apoptotic and late cells increased from 16 h onwards (Fig. 4b).

Mitochondrial membrane potential

In NHLF, when treated with 5 μM of SM, the population of live cells with the depolarized mitochondrial membrane showed a significant increase at 48 and 72 h. The population of depolarized/dead cells was higher at the same time intervals. The concentration of 10 μM raised the amount of depolarized/live cells at 24 and 72 h, while the population of depolarized/dead cells increased at 72 h. At 100 μM, the amount of depolarised/live cells was increased at 8, 36, 48, and 72 h, while the population of depolarised/dead cells was higher at 16, 24, 36, 48, and 72 h. The population of terminally dead cells increased at 48 and 72 h (Fig. 5a).

In A-549 cells, the population of depolarized/dead cells increased at 5 μM at 36, 48 and 72 h. The concentration of 10 μM of SM increased the population of depolarized/dead at the same time intervals. Finally, 100 μM caused a significant rise of depolarized/dead cells from 24 h onwards (Fig. 5b).

Cellular morphology

Pictures from the phase-contrast light microscope showed changes in the morphology of cells treated with 100 μM of SM (Fig. 6). Both types of untreated cells reached confluence during 72 h.

NHLF cells have fibroblast-like morphology. The growth of SM treated cells was inhibited in comparison with control 24 h post-treatment. The progression of morphologic hallmarks of apoptosis occurred at 48 and 72 h.

A-549 cells have an epithelial-like morphology. The SM treated cells started to show a decrease in size and rounding up, with increasing intercellular spaces after 24 h. Similarly to NHLF, the number of shrunk and floating cells was increased at 48 and 72 h. The changes in morphology associated with apoptosis were more pronounced in A-549 cells than in NHLF. Besides apoptosis, morphologically intact cells were founded in both cell lines.

Changes in intracellular ROS level

The generation of intracellular ROS was measured using fluorescent probe DCFH-DA, which non-specifically interacts with different ROS species. When compared with control, we did not observe any induction of ROS in both NHLF (Fig. 7a) and A-549 cells (Fig. 7b).

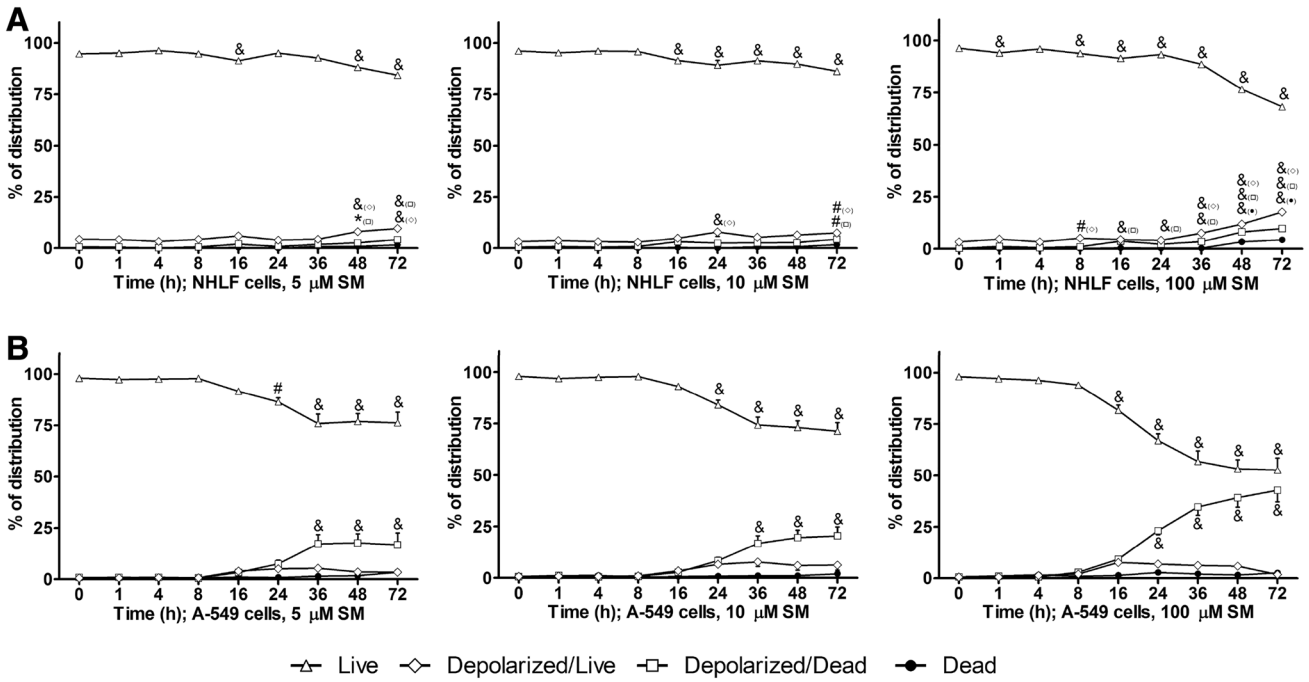

Fig. 5 Time-course of changes in mitochondrial membrane potential induced by SM in (**a**) NHLF and (**b**) A-549 cells. The cells were treated with 5, 10 and 100 μM SM. Measurement of mitochondrial potential was performed at the indicated time by microcapillary flow cytometry. The data are expressed as mean ± SEM from three independent experiments. $^{*}p \leq 0.05$, $^{\#}p \leq 0.01$ and $^{\&}p \leq 0.001$ when compared with the control (0)

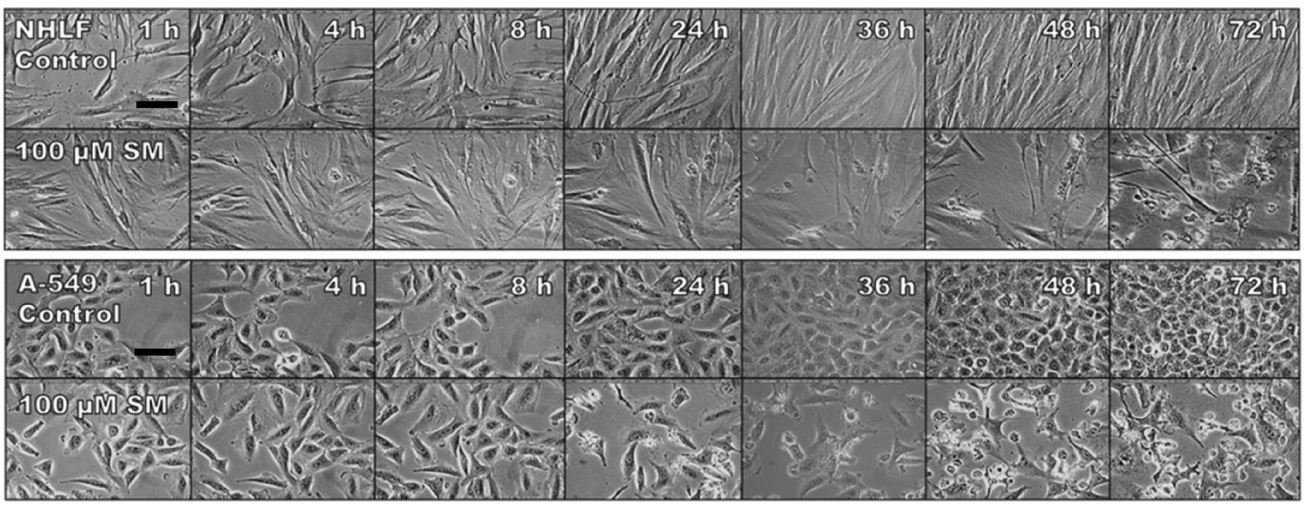

Fig. 6 Morphological changes of NHLF and A-549 cells treated with 100 μM of SM during the 72 h period. Phase-contrast microscopy, magnification × 200. Scale bars represent 100 μm

Tert-butylhydroperoxide at 50, 100 and 200 μM was utilized as a positive control, demonstrating an increase of fluorescence of DCFH-DA with a peak at 4 h after the treatment (Fig. 7c).

Cell cycle distribution

In NHLF cells, the number of cells in S-phase increased, especially at the expense of G_0/G_1 population after the

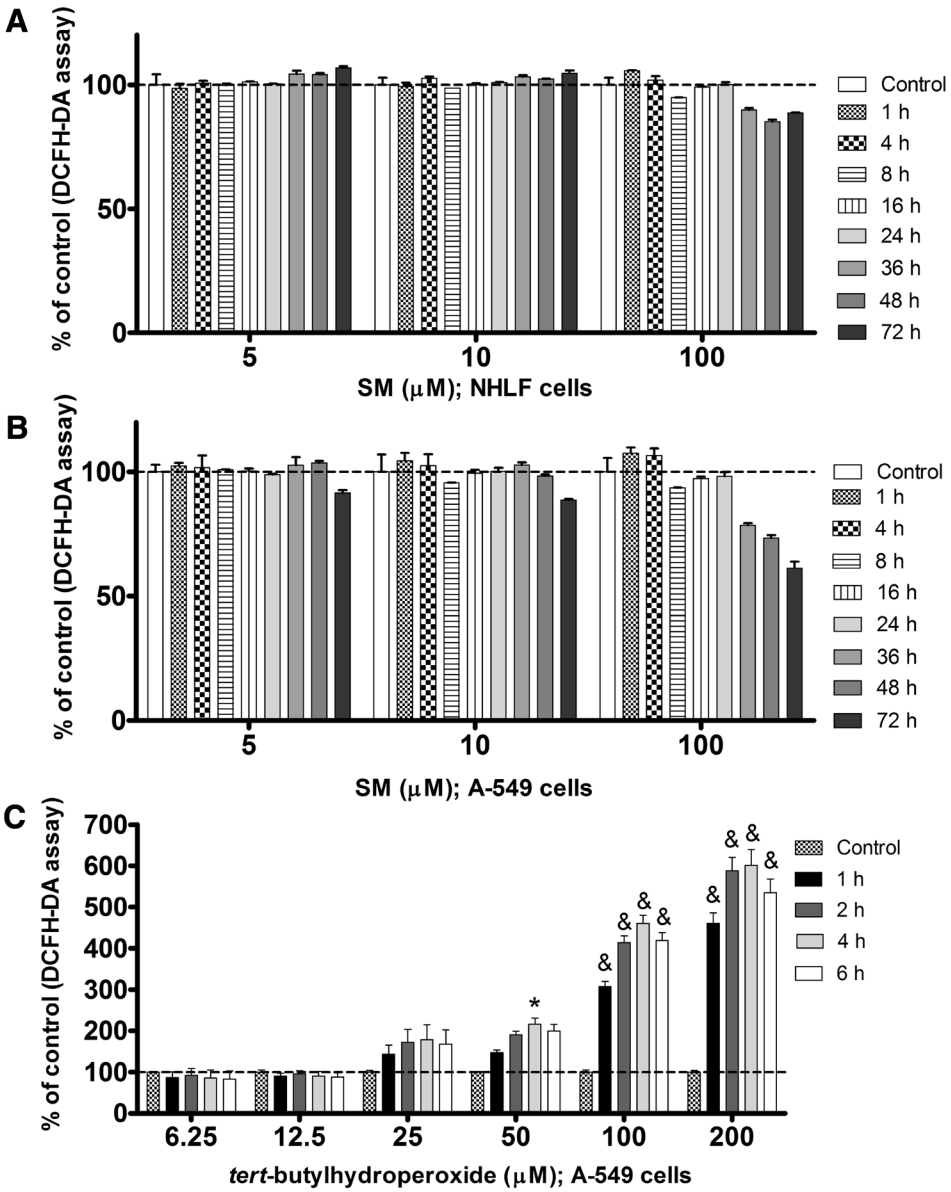

Fig. 7 Time-course of changes in intracellular ROS levels induced by SM in (**a**) NHLF and (**b**) A-549 cells. The cells were treated with 5, 10 and 100 μM of SM and incubated with DCFH-DA. **c** *Tert*-butylhydroperoxide was used as a positive control in A-549 cells. The data are expressed as mean ± SEM, $n = 4$. $^{*}p \leq 0.05$ and $^{\&}p \leq 0.001$ when compared with the control

treatment with 5 μM of SM from 16 h onwards. At the concentration of 10 μM, the percentage of this population was higher at the same time intervals. The concentration of 100 μM SM did not cause any statistically significant changes when compared with control (Fig. 8a).

A-549 cells showed similar trends. At 5 μM of SM, we found a significant increase in S-phase cells from 16 h onwards. At the concentration of 10 μM, the percentage of this population was higher at the same time intervals. At 100 μM, the S-phase population was increased at 72 h (Fig. 8b).

ATM activation

SM did not elicit activation of ATM in NHLF treated by 5 μM SM. At 10 μM, SM increased phosphorylation of ATM at 24 h. The concentration of 100 μM increased the amount of ATM positive cells from 16 h onwards (Fig. 9a).

In A-549 cells, 5 μM of SM increased phosphorylation of ATM at 8 and 72 h. The number of ATM positive cells was higher at 8 h after the 10 μM treatment. SM at the concentration of 100 μM caused a significant increase in this parameter at 4, 8, 16, and 24 h (Fig. 9b).

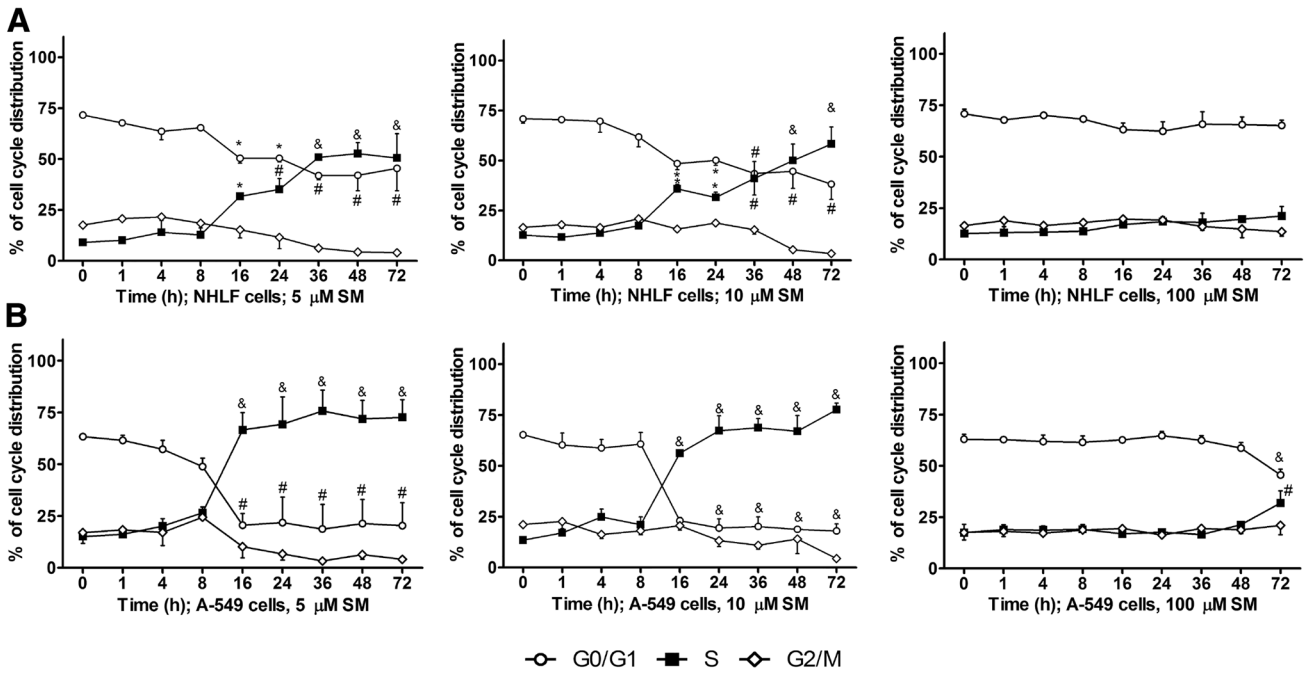

Fig. 8 Time-course of changes in cell cycle distribution induced by SM in (**a**) NHLF and (**b**) A549 cells. The cells were treated with 5, 10 and 100 μM of SM. At the indicated time, ethanol-fixed cells were stained with propidium iodide and analyzed by microcapillary flow cytometry. The data are expressed as mean ± SEM from three independent experiments. $^{*}p \leq 0.05$, $^{\#}p \leq 0.01$ and $^{\&}p \leq 0.001$ when compared with the control (0)

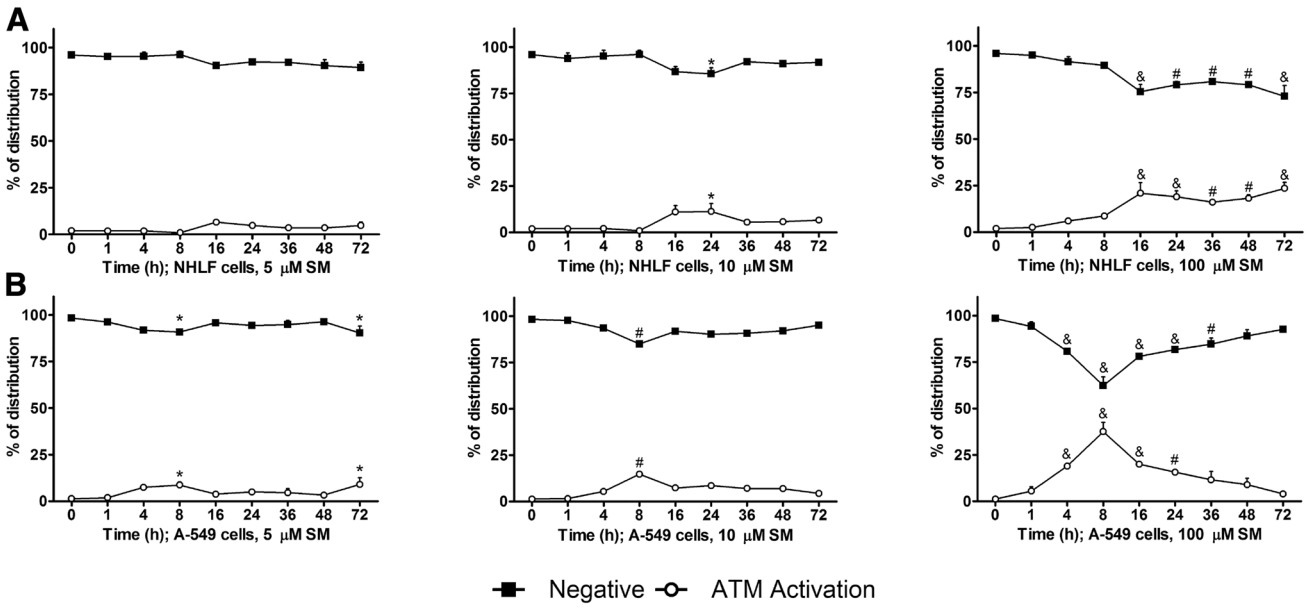

Fig. 9 Time-course of ATM activation (phospho-ATM) induced by SM in (**a**) NHLF and (**b**) A-549 cells. Cells were treated with 5, 10 and 100 μM of SM. At the indicated time, samples for ATM analysis were prepared and analyzed by microcapillary flow cytometry. The data are expressed as mean ± SEM from three independent experiments. $^{*}p \leq 0.05$, $^{\#}p \leq 0.01$ and $^{\&}p \leq 0.001$ when compared with the control (0)

Discussion

The SM toxicity involves complex mechanisms, including DNA alkylation, SM-protein adduct formation, oxidative stress, development of inflammation response, and consequently cell death (Jowsey et al. 2012; Khan et al. 2017). Each of these may impact overall short- or long-term adverse effects. In the present work, we demonstrate a time- and concentration-dependent cytotoxic profile of SM in both human lung fibroblasts NHLF and lung epithelial cells A-549.

The critical event of SM toxicity is DNA alkylation damage (Jowsey et al. 2012; Lüling et al. 2018). Our recently published data demonstrated that DNA cross-links were partially repaired at concentrations lower than 250 µM. Moreover, this process was associated with a decrease in A-549 cell viability (Jost et al. 2015). Based on this, we selected three concentrations of SM (5, 10 and 100 µM) to study time-related cellular responses in detail. At these concentrations, SM produces mono- and bifunctional DNA adducts that interfere with cell cycle progression. Our results show that SM caused an accumulation of cells in the S-phase at concentrations of 5 and 10 µM. This effect was more profound in A-549 than in NHLF. For alkylating agents, S-phase is particularly sensitive. The presence of pathological covalent bonds in double-strand DNA results in a replication fork stalling, activation of ataxia telangiectasia and Rad3-related protein (ATR) and initiation of repair machinery via complex repair mechanism, including homologous recombination (Legerski 2010). The collapse of the replication fork in mammalian cells appears with approximately 12 h delay, depending on the cell type and cross-linking agent (Niedernhofer et al. 2004; Legerski 2010). According to our results, a completely different situation occurred when SM was applied at 100 µM concentration. High levels of DNA alkylation/cross-links seem to paralyze the cell cycle in all phases simultaneously.

Apart from ATR, other phosphatidylinositol 3-kinases, such as ataxia-telangiectasia mutated protein (ATM), can be activated in response to the DNA damage. ATM kinase is particularly sensitive to DNA double-strand breaks (DSBs) (Maréchal and Zou 2013). SM does not induce DSBs directly. They are more likely initiated during repair processes (Debiak et al. 2009). In the S-phase, which is critical for cross-link recognition and repair, DSBs form as an intermediate of the homologous recombination process (Niedernhofer et al. 2004). In our study, SM induced only weak activation of ATM in cells treated with 5 and 10 µM. On the other hand, 100 µM elicited significant activation of ATM. Such damage appears to suppress cell cycle progression in NHLF 16–72 h after the exposure. In A-549 cells, ATM activation was observed only in the 4–48 h intervals. At 72 h, ATM signaling restored to control levels, which correlated with the renewal of cell cycle progression, an increase of cell population in S-phase, and elevation of growth curves measured by electric impedance-based assay.

Oxidative stress is considered as another potent factor of SM toxicity (Naghii 2002; Laskin et al. 2010; Pohanka et al. 2017). In vitro, the generation of oxidative stress by SM was demonstrated at 50 µM using DCFH-DA fluorescence probe in human fetal hepatocyte L02 cells (Zhang et al. 2019). In another study, Long et al. (2016) described a significant decrease of glutathione and a considerable increase in the reactive oxygen and nitrogen species (RONS) levels in HEK-f cells 2 h after exposure to 300 µM SM. Long et al. (2016) utilized CM-H_2DCFDA probe, a chloromethyl derivate of H_2DCF-DA, which exhibits better retention in live cells. Both studies are in contrast with our results. We did not find any significant changes in ROS levels measured by DCFH-DA probe. It seems that the induction of oxidative stress by SM is dependent on the selected cellular model and/or experimental design.

A permeation of mitochondria and the decline of transmembrane mitochondrial potential is one of the first hallmarks of apoptosis. This process is associated with the opening of mitochondrial permeability transition pores followed by depolarization of transmembrane potential and loss of oxidative phosphorylation (Ly et al. 2003). Our results indicate that SM elicits a mitochondrial dysfunction related to depolarization of the mitochondrial membrane. It also corresponds to the study by Long et al. (2016) who observed depolarization of mitochondrial membrane in a concentration-dependent manner in HEK-f cells exposed to SM at 100, 300 and 450 µM. A similar effect was described in SAE and 16HBE cells treated by 2-chloroethyl ethyl sulfide (CEES) (Gould et al. 2009). Our results show that A-549 cells are more susceptible to mitochondria damage than NHLF. Gould et al. (2009) proposed that CEES or SM may act as an uncoupling agent of the mitochondrial respiratory chain, producing oxidative stress. However, our results do not support this hypothesis.

A release of apoptogenic factor, cytochrome C, follows the depolarization of the mitochondrial membrane. This factor activates caspases, including effector caspase-3 and -7, which cleave hundreds of cellular proteins. Flippases are one of their targets. In healthy cells, flippases confine nearly all phosphatidylserine (and other aminophospholipids) to the inner leaflet of the plasma membrane. When apoptosis is triggered, caspases inactivate flippases, allowing phosphatidylserine to be distributed into the outer leaflet of the plasma membrane (Rysavy et al. 2014). The annexin-V antibody can detect externalization of phosphatidylserine. It is a feature characteristic for an early stage of apoptosis, in which the integrity of the

cytoplasmatic membrane is not yet compromised. The subsequent phase, late apoptosis, displays the permeabilization of plasmatic membranes. The cells then become positive for both annexin-V and PI. But when cells are positive solely for PI they are considered necrotic. SM induces predominantly apoptotic cell death and only a low level of necrosis is detected under in vitro conditions (Kehe et al. 2000). This corresponds to our findings. It is, however, noteworthy that the activation of apoptosis directly followed the depolarization of the mitochondrial membrane in A-549 cells, while we observed a specific latency between both processes in NHLF cells. It seems that after SM treatment, NHLF activates a mechanism delaying the progress of apoptosis.

In our study, we also utilized another three methods to investigated changes in cell viability, including fluorescence-based calcein-AM assay, MTT reduction assay and real-time electro-impedance cell analysis. The fluorescence-based calcein-AM test evaluates changes in the permeability of the cell membrane. This assay distinguishes live cells according to the presence of ubiquitous intracellular esterases, which convert the nonfluorescent cell-permeant calcein-AM to the intensely green fluorescent nonpermeable calcein (Gao et al. 2007). The results timely correlated with the increase of cell permeability measured using annexin V/PI and with cellular morphology changes observed using a phase-contrast light microscope at 100 µM SM.

MTT reduction assay evaluates a rate of the glycolytic NAD(P)H production together with the activity of other glycolytic enzymes of the endoplasmatic reticulum. Nevertheless, the NAD(P)H coenzyme is mainly responsible for the conversion of MTT salt to formazan (Stockert et al. 2018). MTT assay confirms the higher susceptibility of A-549 to SM-induced damage. In both cell lines, the decrease of values also preceded the depolarization of the mitochondrial membrane and the apoptotic process. SM significantly interferes with energetic metabolism. A possible explanation may, therefore, lay in overactivation of poly(ADP-ribose) polymerase in response to DNA damage, inhibition of glycolysis and depletion of substrates such as NAD^+ (Ruszkiewicz et al. 2020).

Real-time electro-impedance cell analysis monitors viability via changes in cell morphology and contact of cells with the surface. The electric signal expressed as dimensionless unit NCI was measured in specially designed 96-well microtiter plate with integrated gold microelectrodes array in the button of each well. Cells growing on the surface of the electrode cover the array and the signal grow up. When the cells stop their growth or die, the signal remains constant or goes down (Kustermann et al. 2013). Both cells display latency of SM toxicity. In NHLF cells, we observed a triphasic response with an increase of NCI during the first phase. Due to the cell cycle arrest, the possible explanation can be associated with cell enlargement. It seems that SM may induce reorganization of the cytoskeleton, leading to cell spreading and increase of NCI signal. Long et al. (2016) found a similar effect. They observed cell swelling and loosening of actin and α-tubulin in HDF-a fibroblast cells treated with 300 µM SM. These facts together implicate that the early stage of SM toxicity is accompanied by unfavorable changes in cytoskeleton, especially in fibroblasts. A-549 cells did not show such an effect. Remarkable is also a phenomenon found at 100 µM SM during long-term incubation. Surviving cells were able to restore their proliferation. Being less sensitive to SM, NHLF cells restored their growth more markedly. The exponential phase of their proliferation observed 5–7 days post-treatment had a similar trend as untreated cells with similar NCI values during the log phase. On the other hand, the proliferation capacity of A-549 did not achieve such progress in the recovery period, indicating the persistence of SM-induced DNA damage.

In conclusion, we compared the cellular stress response of NHLF and A-549 cells after SM treatment. Changes in both cell lines were distinctive with the latency for several hours. The results indicate that NHLF cells are less prone to toxic damage induced by SM in terms of losing transmembrane mitochondrial potential, activating the apoptosis and losing cell viability. SM interferes in the cell cycle and causes S-phase arrest at low concentration. We did not confirm the direct generation of ROS in our experiments despite changes in the cellular antioxidant system have been known. We also revealed a remarkable cell recovery during long-term incubation in both cell lines. This work provides a detailed time-related cytotoxic profile of A-549 and NHLF cells for future investigation of prevention and/or mitigation of SM-induced toxic effects. Further studies are particularly necessary to characterize the cell recovery process from acute SM toxicity and long-term toxic effects.

Acknowledgements This work was funded by a long-term organization development plan—Medical Aspects of Weapons of Mass Destruction of the Faculty of Military Health Sciences, University of Defence in Brno.

Author contributions Conceived of or designed the study: PJ, JP, Performed research: PJ, LM, Analyzed data: PJ, LM, Contributed new methods or models: PJ, Wrote the paper: PJ, JP.

Compliance with ethical standards

Conflict of interest The authors declare that they have no conflict of interest.

References

Debiak M, Kehe K, Bürkle A (2009) Role of poly(ADP-ribose) polymerase in sulfur mustard toxicity. Toxicology 263:20–25. https://doi.org/10.1016/j.tox.2008.06.002

Gao X, Ray R, Xiao Y et al (2007) Inhibition of sulfur mustard-induced cytotoxicity and inflammation by the macrolide antibiotic roxithromycin in human respiratory epithelial cells. BMC Cell Biol 8:17. https://doi.org/10.1186/1471-2121-8-17

Gould NS, White CW, Day BJ (2009) A role for mitochondrial oxidative stress in sulfur mustard analog 2-chloroethyl ethyl sulfide-induced lung cell injury and antioxidant protection. J Pharmacol Exp Ther 328:732–739. https://doi.org/10.1124/jpet.108.145037

Imani S, Panahi Y, Salimian J et al (2015) Epigenetic: a missing paradigm in cellular and molecular pathways of sulfur mustard lung: a prospective and comparative study. Iran J Basic Med Sci 18:723–736

Inturi S, Tewari-Singh N, Gu M et al (2011) Mechanisms of sulfur mustard analog 2-chloroethyl ethyl sulfide-induced DNA damage in skin epidermal cells and fibroblasts. Free Radic Biol Med 51:2272–2280. https://doi.org/10.1016/j.freeradbiomed.2011.08.020

Jost P, Svobodova H, Stetina R (2015) Induction and repair of DNA cross-links induced by sulfur mustard in the A-549 cell line followed by a comet assay. Chem Biol Interact 237:31–37. https://doi.org/10.1016/j.cbi.2015.05.009

Jowsey PA, Williams FM, Blain PG (2012) DNA damage responses in cells exposed to sulphur mustard. Toxicol Lett 209:1–10. https://doi.org/10.1016/j.toxlet.2011.11.009

Kehe K, Reisinger H, Szinicz L (2000) Sulfur mustard induces apoptosis and necrosis in SCL II cells in vitro. J Appl Toxicol JAT 20(Suppl 1):S81–86. https://doi.org/10.1002/1099-1263(200012)20:1+<:aid-jat684>3.0.co;2-k

Khan F, Niaz K, Ismail Hassan F, Abdollahi M (2017) An evidence-based review of the genotoxic and reproductive effects of sulfur mustard. Arch Toxicol 91:1143–1156. https://doi.org/10.1007/s00204-016-1911-8

Kustermann S, Boess F, Buness A et al (2013) A label-free, impedance-based real time assay to identify drug-induced toxicities and differentiate cytostatic from cytotoxic effects. Toxicol In Vitro 27:1589–1595. https://doi.org/10.1016/j.tiv.2012.08.019

Laskin JD, Black AT, Jan Y-H et al (2010) Oxidants and antioxidants in sulfur mustard–induced injury. Ann N Y Acad Sci 1203:92–100. https://doi.org/10.1111/j.1749-6632.2010.05605.x

Legerski RJ (2010) Repair of DNA interstrand cross-links during S phase of the mammalian cell cycle. Environ Mol Mutagen 51:540–551. https://doi.org/10.1002/em.20566

Long L, Li W, Chen W et al (2016) Dynamic cytotoxic profiles of sulfur mustard in human dermal cells determined by multiparametric high-content analysis. Toxicol Res 5:583–593. https://doi.org/10.1039/C5TX00305A

Lüling R, John H, Gudermann T et al (2018) Transient receptor potential channel A1 (TRPA1) regulates sulfur mustard-induced expression of heat shock 70 kDa Protein 6 (HSPA6) In Vitro. Cells 7:2–19. https://doi.org/10.3390/cells7090126

Ly JD, Grubb DR, Lawen A (2003) The mitochondrial membrane potential [deltapsi(m)] in apoptosis; an update. Apoptosis Int J Program Cell Death 8:115–128. https://doi.org/10.1023/a:1022945107762

Maréchal A, Zou L (2013) DNA damage sensing by the ATM and ATR Kinases. Cold Spring Harb Perspect Biol 5:34–97. https://doi.org/10.1101/cshperspect.a012716

Naghii MR (2002) Sulfur mustard intoxication, oxidative stress, and antioxidants. Mil Med 167:573–575

Niedernhofer LJ, Odijk H, Budzowska M et al (2004) The structure-specific endonuclease Ercc1-Xpf Is required to resolve DNA interstrand cross-link-induced double-strand breaks. Mol Cell Biol 24:5776. https://doi.org/10.1128/MCB.24.13.5776-5787.2004

Pilatte E, Lison D (1994) Effects of sulfur mustard on selected biochemical parameters of murine peritoneal macrophages in culture. Toxicol In Vitro 8:125–130. https://doi.org/10.1016/0887-2333(94)90216-X

Pohanka M, Martinkova P, Brtnicky M, Kynicky J (2017) Changes in the oxidative stress/antioxidant system after exposure to sulfur mustard and antioxidant strategies in the therapy, a review. Toxicol Mech Methods 27:408–416. https://doi.org/10.1080/15376516.2017.1320695

Ruszkiewicz JA, Bürkle A, Mangerich A (2020) NAD+ in sulfur mustard toxicity. Toxicol Lett 324:95–103. https://doi.org/10.1016/j.toxlet.2020.01.024

Rysavy NM, Shimoda LMN, Dixon AM et al (2014) Beyond apoptosis: the mechanism and function of phosphatidylserine asymmetry in the membrane of activating mast cells. Bioarchitecture 4:127–137. https://doi.org/10.1080/19490992.2014.995516

Sawyer TW, Nelson P, Bjarnason S et al (2010) Ionic dependence of sulphur mustard cytotoxicity. Toxicol Appl Pharmacol 247:179–190. https://doi.org/10.1016/j.taap.2010.06.010

Seagrave J, Weber WM, Grotendorst GR (2010) Sulfur mustard vapor effects on differentiated human lung cells. Inhal Toxicol 22:896. https://doi.org/10.3109/08958378.2010.493901

Stockert JC, Horobin RW, Colombo LL, Blázquez-Castro A (2018) Tetrazolium salts and formazan products in cell biology: viability assessment, fluorescence imaging, and labeling perspectives. Acta Histochem 120:159–167. https://doi.org/10.1016/j.acthis.2018.02.005

Tewari-Singh N, Gu M, Agarwal C et al (2010) Biological and molecular mechanisms of sulfur mustard analog-induced toxicity in JB6 and HaCaT cells: possible role of ATM/ATR-cell cycle checkpoint pathway. Chem Res Toxicol 23:1034–1044. https://doi.org/10.1021/tx100038b

Weinberger B, Laskin JD, Sunil V et al (2011) Sulfur mustard-induced pulmonary injury: therapeutic approaches to mitigating toxicity. Pulm Pharmacol Ther 24:92–99. https://doi.org/10.1016/j.pupt.2010.09.004

Zhang H, Chen Y, Pei Z et al (2019) Protective effects of polydatin against sulfur mustard-induced hepatic injury. Toxicol Appl Pharmacol 367:1–11. https://doi.org/10.1016/j.taap.2019.01.013